

Explaining the possible 95 GeV excesses in the B-L symmetric SSM

Jin-Lei Yang^{1,2,3*}, Ming-Hui Guo^{1,2}, Wen-Hui

Zhang^{1,2}, Hai-Bin Zhang^{1,2,3†}, Tai-Fu Feng^{1,2,3‡}

Department of Physics, Hebei University, Baoding, 071002, China¹

Hebei Key Laboratory of High-precision Computation and

Application of Quantum Field Theory, Baoding, 071002, China²

Hebei Research Center of the Basic Discipline for

Computational Physics, Baoding, 071002, China³

Abstract

Motivated by the excesses around 95 GeV observed in the diphoton and $b\bar{b}$ data, this study focuses on investigating these two excesses within the framework of the $B - L$ supersymmetric model (B-LSSM), due to the existence of two light Higgs bosons in the model. Considering the two-loop effective potential corrections, it is found that the B-LSSM is hard to fit the 125 GeV Higgs signal strengths and the two excesses around 95 GeV in the experimental 1σ intervals, while the model can reproduce them in the experimental 2σ intervals simultaneously. And considering the two loop effective potential corrections to the squared Higgs mass matrix is important to account for the mixing effects among Higgs sector.

Keywords: Higgs signals, 95 excesses, new Higgs states

* jlyang@hbu.edu.cn

† hbzhang@hbu.edu.cn

‡ fengtf@hbu.edu.cn

Identifying whether the detected Higgs boson is the only fundamental scalar particle or part of a new physics (NP) theory with extended Higgs sectors is the prime goal of the current LHC programme. Although there is no new scalar was found at the LHC so far, several intriguing excesses in the searches for light Higgs bosons below 125 GeV have been observed with increasing precision in the measurements of Higgs couplings to fermions and gauge bosons. The results based on both the CMS Run 1 and the first year of CMS Run 2 data for Higgs boson searches in the diphoton final state show a 2.8σ local excess at the mass about 95 GeV [1, 2], which is compatible with the latest ATLAS result [3] based on the previously reported result utilizing 80 fb^{-1} [4] in the diphoton searches

$$\mu(\Phi_{95})_{\gamma\gamma} = \frac{\sigma(gg \rightarrow \Phi_{95}^{\text{NP}})\text{BR}(\Phi_{95}^{\text{NP}} \rightarrow \gamma\gamma)}{\sigma(gg \rightarrow h_{95}^{\text{SM}})\text{BR}(h_{95}^{\text{SM}} \rightarrow \gamma\gamma)} = 0.18 \pm 0.10. \quad (1)$$

Utilizing the full Run 2 data set, CMS published the results for the Higgs boson searches in the $\tau^+\tau^-$ channel which show a local significance of 3.1σ at a mass value about 95 GeV [5]

$$\mu(\Phi_{95})_{\tau\tau} = \frac{\sigma(gg \rightarrow \Phi_{95}^{\text{NP}})\text{BR}(\Phi_{95}^{\text{NP}} \rightarrow \tau\tau)}{\sigma(gg \rightarrow h_{95}^{\text{SM}})\text{BR}(h_{95}^{\text{SM}} \rightarrow \tau\tau)} = 1.2 \pm 0.5. \quad (2)$$

The analysis on the Higgs boson searches in the diphoton final state by CMS further confirmed the excess at about 95 GeV, and the result reads [6]

$$\mu(\Phi_{95})_{\gamma\gamma} = 0.33^{+0.19}_{-0.12}. \quad (3)$$

In addition, the results measured at the Large Electron Positron (LEP) show a local excess of 2.3σ at the invariant mass of $b\bar{b}$ around 98 GeV¹ [7], which can be expressed in terms of a signal strength as

$$\mu(\Phi_{95})_{b\bar{b}} = 0.117 \pm 0.057. \quad (4)$$

Theoretically, there are numerous discussions on the excesses in NP models. The analysis carried out in Refs. [8–24] indicates that the diphoton rate may be several times larger than its SM prediction for the same scalar mass in the next-to-minimal supersymmetric standard

¹ The excess at LEP is broad due to the hadronic $b\bar{b}$ final state, so this result is also compatible with a scalar resonance at 95 GeV, consistent with the diphoton and ditau excesses. We also take the excess for $b\bar{b}$ final state at about 95 GeV in the following analysis.

model (NMSSM). In the Two-Higgs doublet model (2HDM) with an additional real singlet (N2HDM), the possibilities of explaining the observed excesses were studied in Refs. [25–33]. The authors of Ref. [34] explored the viability of the radion mixed Higgs to be 125 GeV along with the presence of a light radion which can account for the CMS diphoton excess well in the Higgs radion mixing model. Considering the one-loop corrections to the neutral scalar masses of the $\mu\nu$ SSM, the authors of Refs. [35, 36] demonstrated how the $\mu\nu$ SSM can simultaneously accommodate two excesses measured at the LEP and LHC at the 1σ level. Based on the analysis in Ref. [37], extending the scalar sector with a $SU(2)_L$ triplet (the hypercharge $Y = 0$) can well provide the origin of the 95 GeV excesses. Whether certain model realizations could simultaneously explain the two excesses while being in agreement with all other Higgs boson related limits and measurements was reviewed in Refs. [38, 39].

In this work, we investigate whether the $B - L$ supersymmetric model (B-LSSM) [40–49] can account for the diphoton and $b\bar{b}$ excesses². Compared with the minimal supersymmetric standard model (MSSM), the gauge symmetry of the B-LSSM is extended by an additional $U(1)_{B-L}$ gauge group, i.e. the full gauge structure is $SU(3)_C \otimes SU(2)_L \otimes U(1)_Y \otimes U(1)_{B-L}$. In addition to the MSSM superfields, two singlet chiral Higgs with nonzero $U(1)_{B-L}$ charge are introduced in the B-LSSM

$$\begin{aligned} H_d &= \begin{pmatrix} H_d^1 \\ H_d^2 \end{pmatrix} \sim (1, 2, -1/2, 0), \quad H_u = \begin{pmatrix} H_u^1 \\ H_u^2 \end{pmatrix} \sim (1, 2, 1/2, 0), \\ \eta &\sim (1, 1, 0, -1), \quad \bar{\eta} \sim (1, 1, 0, 1), \end{aligned} \quad (5)$$

where the charges in the brackets correspond to $SU(3)_C$, $SU(2)_L$, $U(1)_Y$, $U(1)_{B-L}$ respectively. The local gauge symmetry $SU(2)_L \otimes U(1)_Y \otimes U(1)_{B-L}$ breaks down to the electromagnetic symmetry $U(1)_{\text{em}}$ as the Higgs fields receive nonzero vacuum expectation values (VEV):

$$\begin{aligned} H_d^1 &= \frac{1}{\sqrt{2}}(v_d + \phi_d + i\sigma_d), & H_u^2 &= \frac{1}{\sqrt{2}}(v_u + \phi_u + i\sigma_u), \\ \eta &= \frac{1}{\sqrt{2}}(u_\eta + \phi_\eta + i\sigma_\eta), & \bar{\eta} &= \frac{1}{\sqrt{2}}(u_{\bar{\eta}} + \phi_{\bar{\eta}} + i\sigma_{\bar{\eta}}). \end{aligned} \quad (6)$$

² Eq. (2) shows obviously that the ditau excess has large experimental uncertainties, combined with the analysis in Ref. [50] which indicates the CP-even dominated Higgs state has difficulties in describing the ditau excess, we focus on the diphoton and $b\bar{b}$ excesses in this work.

For convenience, we can define $v^2 = v_d^2 + v_u^2$, $u^2 = u_\eta^2 + u_{\bar{\eta}}^2$, $\tan \beta = v_u/v_d$, $\tan \beta' = u_{\bar{\eta}}/u_\eta$. The tree-level scalar potential in the B-LSSM can be written as [51]

$$\begin{aligned} V^{(0)} = & (m_{H_d}^2 + \mu^2)H_d^2 + (m_{H_u}^2 + \mu^2)H_u^2 + (m_\eta^2 + \mu_\eta^2)\eta^2 + (m_{\bar{\eta}}^2 + \mu_{\bar{\eta}}^2)\bar{\eta}^2 \\ & - 2B_\mu H_d H_u - 2B_\eta \eta \bar{\eta} + \frac{1}{8}(g_1^2 + g_2^2 + g_{YB}^2)(H_d^2 - H_u^2)^2 + \frac{1}{2}g_B^2(\eta^2 - \bar{\eta}^2)^2 \\ & + \frac{1}{2}g_B g_{YB}(H_d^2 - H_u^2)(\eta^2 - \bar{\eta}^2), \end{aligned} \quad (7)$$

where g_B is the gauge coupling constant corresponding to the $U(1)_{B-L}$ gauge group, g_{YB} is the coupling constant arising from the kinetic mixing effect. For the one-loop and two-loop effective potential, the dominant contributions come from top and stop quarks. In the B-LSSM, the top quark mass reads

$$m_t = \frac{1}{\sqrt{2}}Y_t v_u. \quad (8)$$

The stop quark mass matrix can be written as

$$m_t^2 = \begin{pmatrix} m_{tL}^2, & \frac{Y_t}{\sqrt{2}}(v_u A_t - v_d \mu) \\ \frac{Y_t}{\sqrt{2}}(v_u A_t - v_d \mu), & m_{tR}^2 \end{pmatrix}, \quad (9)$$

where

$$\begin{aligned} m_{tL}^2 = & \frac{1}{24}[(g_1^2 - 3g_2^2 + g_{YB}^2 + g_B g_{YB})(v_u^2 - v_d^2) + 2g_B(g_B + g_{YB})(u_\eta^2 - u_{\bar{\eta}}^2)] \\ & + m_{\tilde{q}}^2 + \frac{1}{2}v_u^2 Y_t^2, \\ m_{tR}^2 = & \frac{1}{24}[(4g_1^2 + 4g_{YB}^2 + g_B g_{YB})(v_d^2 - v_u^2) + 2g_B(g_B + 4g_{YB})(u_\eta^2 - u_{\bar{\eta}}^2)] \\ & + m_{\tilde{u}}^2 + \frac{1}{2}v_u^2 Y_t^2. \end{aligned} \quad (10)$$

On the mass eigenstates, the physical stop masses can be written as

$$M_{t1,2}^2 = \frac{1}{2}(m_{tL}^2 + m_{tR}^2) \pm \left[\frac{1}{4}(m_{tL}^2 - m_{tR}^2)^2 + \frac{1}{2}Y_t^2(v_u A_t - v_d \mu)^2 \right]^{1/2}. \quad (11)$$

The effective potential is

$$V_{\text{eff}} = V^{(0)} + \Delta V = V^{(0)} + V^{(1)} + V^{(2)}, \quad (12)$$

where $V^{(1)}$, $V^{(2)}$ denote the one-loop and two-loop effective potential respectively [52–54]

$$\begin{aligned}
V^{(1)} &= -\frac{3}{16\pi^2}(m_t^2)^2(\log \frac{m_t^2}{Q^2} - \frac{3}{2}) + \frac{3}{32\pi^2} \sum_{i=1}^2 (M_{t_i}^2)^2(\log \frac{M_{t_i}^2}{Q^2} - \frac{3}{2}), \\
V^{(2)} &= \frac{\alpha_s}{16\pi^3} \left\{ 2J(m_t^2, m_t^2) - 4m_t^2 I(m_t^2, m_t^2, 0) + [2M_{t_1}^2 I(M_{t_1}^2, M_{t_1}^2, 0) + 2L(M_{t_1}^2, M_{\tilde{g}}^2, m_t^2) \right. \\
&\quad - 4m_t M_{\tilde{g}} S_{2\bar{\theta}} I(M_{t_1}^2, M_{\tilde{g}}^2, m_t^2) + \frac{1}{2}(1 + 2C_{2\bar{\theta}}^2)J(M_{t_1}^2, M_{t_1}^2) + \frac{S_{2\bar{\theta}}^2}{2}J(M_{t_1}^2, M_{t_2}^2) \\
&\quad \left. + (M_{t_1} \leftrightarrow M_{t_2}, S_{2\bar{\theta}} \leftrightarrow -S_{2\bar{\theta}})] \right\}'' \quad (13)
\end{aligned}$$

In Eq. (13), $M_{\tilde{g}}$ is the mass of sgluon and

$$S_{2\bar{\theta}} = \frac{2(M_{\tilde{t}})_{12}}{M_{t_1}^2 - M_{t_2}^2}, \quad (14)$$

where $(M_{\tilde{t}})_{12} = Y_t(v_u A_t - v_d \mu)$. For the two-loop functions I , J in Eq. (13) can be found in the appendix D of Ref. [55].

Taking into account the the vacuum stability conditions, we can obtain the elements of the CP-even Higgs squared mass matrix

$$\begin{aligned}
m_{\phi_d \phi_d}^2 &= \frac{1}{4}(g_1^2 + g_2^2 + g_{YB}^2)v_d^2 + B_\mu v_u/v_d + \left[-\frac{1}{\phi_d} \frac{\partial \Delta V}{\partial \phi_d} + \frac{\partial^2 \Delta V}{\partial \phi_d \partial \phi_d} \right]_{\text{VEV}}, \\
m_{\phi_d \phi_u}^2 &= m_{\phi_u \phi_d}^2 = -B_\mu - \frac{1}{4}(g_1^2 + g_2^2 + g_{YB}^2)v_d v_u + \left[\frac{\partial^2 \Delta V}{\partial \phi_d \partial \phi_u} \right]_{\text{VEV}}, \\
m_{\phi_d \phi_\eta}^2 &= m_{\phi_\eta \phi_d}^2 = \frac{1}{2}g_B g_{YB} v_d v_\eta + \left[\frac{\partial^2 \Delta V}{\partial \phi_d \partial \phi_\eta} \right]_{\text{VEV}}, \\
m_{\phi_d \phi_{\bar{\eta}}}^2 &= m_{\phi_{\bar{\eta}} \phi_d}^2 = -\frac{1}{2}g_B g_{YB} v_d v_{\bar{\eta}} + \left[\frac{\partial^2 \Delta V}{\partial \phi_d \partial \phi_{\bar{\eta}}} \right]_{\text{VEV}}, \\
m_{\phi_u \phi_u}^2 &= \frac{1}{4}(g_1^2 + g_2^2 + g_{YB}^2)v_u^2 + B_\mu v_d/v_u + \left[-\frac{1}{\phi_u} \frac{\partial \Delta V}{\partial \phi_u} + \frac{\partial^2 \Delta V}{\partial \phi_u \partial \phi_u} \right]_{\text{VEV}}, \\
m_{\phi_u \phi_\eta}^2 &= m_{\phi_\eta \phi_u}^2 = -\frac{1}{2}g_B g_{YB} v_u v_\eta + \left[\frac{\partial^2 \Delta V}{\partial \phi_u \partial \phi_\eta} \right]_{\text{VEV}}, \\
m_{\phi_u \phi_{\bar{\eta}}}^2 &= m_{\phi_{\bar{\eta}} \phi_u}^2 = \frac{1}{2}g_B g_{YB} v_u v_{\bar{\eta}} + \left[\frac{\partial^2 \Delta V}{\partial \phi_u \partial \phi_{\bar{\eta}}} \right]_{\text{VEV}}, \\
m_{\phi_\eta \phi_\eta}^2 &= g_B^2 v_\eta^2 + B_\eta v_{\bar{\eta}}/v_\eta + \left[-\frac{1}{\phi_\eta} \frac{\partial \Delta V}{\partial \phi_\eta} + \frac{\partial^2 \Delta V}{\partial \phi_\eta \partial \phi_\eta} \right]_{\text{VEV}}, \\
m_{\phi_\eta \phi_{\bar{\eta}}}^2 &= m_{\phi_{\bar{\eta}} \phi_\eta}^2 = -B_\eta - g_B^2 v_\eta v_{\bar{\eta}} + \left[\frac{\partial^2 \Delta V}{\partial \phi_\eta \partial \phi_{\bar{\eta}}} \right]_{\text{VEV}}, \\
m_{\phi_{\bar{\eta}} \phi_{\bar{\eta}}}^2 &= g_B^2 v_{\bar{\eta}}^2 + B_\eta v_\eta/v_{\bar{\eta}} + \left[-\frac{1}{\phi_{\bar{\eta}}} \frac{\partial \Delta V}{\partial \phi_{\bar{\eta}}} + \frac{\partial^2 \Delta V}{\partial \phi_{\bar{\eta}} \partial \phi_{\bar{\eta}}} \right]_{\text{VEV}}, \quad (15)
\end{aligned}$$

To illustrate clearly that there are two light Higgs bosons in the B-LSSM, we calculate the eigenvalues of the tree-level squared Higgs mass matrix under the approximation $v^2 \ll u^2$, the analytical results can be written as

$$\begin{aligned} m_{h_1, \text{tree}}^2 &\approx \frac{2B_\eta(\tan^2 \beta' - 1)^2}{1 + (\tan^2 \beta' + 1)B_\eta/(g_B^2 u^2)}, & m_{h_2, \text{tree}}^2 &\approx \frac{(g_1^2 + g_2^2 + g_{YB}^2)(\tan^2 \beta - 1)^2 v^2}{4(\tan^2 \beta + 1)^2}, \\ m_{h_3, \text{tree}}^2 &\approx \frac{B_\mu}{\tan \beta}(\tan^2 \beta + 1), & m_{h_4, \text{tree}}^2 &\approx 2\left(\frac{g_B^2 u^2}{\tan^2 \beta + 1} + B_\eta\right), \end{aligned} \quad (16)$$

where the terms proportional to $\mathcal{O}[(\tan^2 \beta' - 1)^3]$ are neglected for simplicity, $m_{h_1, \text{tree}}$, $m_{h_4, \text{tree}}$ are the tree-level masses of the states dominated by the two specific scalar singlets in the B-LSSM, and $m_{h_2, \text{tree}}$, $m_{h_3, \text{tree}}$ are the tree-level masses of the states dominated by the two scalar doublets which correspond to the two scalar doublets in the MSSM. As shown in Eq. (16), $m_{h_2, \text{tree}}$ corresponds to the mass of SM-like Higgs, and $m_{h_3, \text{tree}} \approx m_A \gtrsim 1 \text{ TeV}$ [56] with m_A denoting the CP-odd Higgs mass in the MSSM, which also indicates the 95 GeV Higgs can not be achieved in the MSSM [57]. $m_{h_1, \text{tree}}$ in Eq. (16) is the other light Higgs in the B-LSSM, its mass can be set around 95 GeV to explain the observed excesses.

On the basis $(\phi_d, \phi_u, \phi_\eta, \phi_{\bar{\eta}})$, the squared mass matrix of CP-even Higgs can be written as

$$M_\phi^2 = \begin{pmatrix} m_{\phi_d \phi_d}^2 & m_{\phi_d \phi_u}^2 & m_{\phi_d \phi_\eta}^2 & m_{\phi_d \phi_{\bar{\eta}}}^2 \\ m_{\phi_d \phi_u}^2 & m_{\phi_u \phi_u}^2 & m_{\phi_u \phi_\eta}^2 & m_{\phi_u \phi_{\bar{\eta}}}^2 \\ m_{\phi_d \phi_\eta}^2 & m_{\phi_u \phi_\eta}^2 & m_{\phi_\eta \phi_\eta}^2 & m_{\phi_\eta \phi_{\bar{\eta}}}^2 \\ m_{\phi_d \phi_{\bar{\eta}}}^2 & m_{\phi_u \phi_{\bar{\eta}}}^2 & m_{\phi_\eta \phi_{\bar{\eta}}}^2 & m_{\phi_{\bar{\eta}} \phi_{\bar{\eta}}}^2 \end{pmatrix}. \quad (17)$$

The squared mass matrix M_ϕ^2 can be diagonalized by the unitary matrix Z_h as

$$\text{diag}(m_{h_1}^2, m_{h_2}^2, m_{h_3}^2, m_{h_4}^2) = Z_h \cdot M_\phi^2 \cdot Z_h^\dagger, \quad (18)$$

where h_i , ($i = 1, 2, 3, 4$) denote the mass eigenstates.

As defined in the introduction sector, the diphoton and $b\bar{b}$ signal strength are

$$\begin{aligned} \mu(h_{95})_{\gamma\gamma} &= \frac{\sigma(gg \rightarrow h_{95}^{\text{NP}}) \text{BR}(h_{95}^{\text{NP}} \rightarrow \gamma\gamma)}{\sigma(gg \rightarrow h_{95}^{\text{SM}}) \text{BR}(h_{95}^{\text{SM}} \rightarrow \gamma\gamma)}, \\ \mu(h_{95})_{b\bar{b}} &= \frac{\Gamma(h_{95}^{\text{NP}} \rightarrow ZZ^*) \text{BR}(h_{95}^{\text{NP}} \rightarrow b\bar{b})}{\Gamma(h_{95}^{\text{SM}} \rightarrow ZZ^*) \text{BR}(h_{95}^{\text{SM}} \rightarrow b\bar{b})}, \end{aligned} \quad (19)$$

where [58]

$$\begin{aligned}\Gamma_{\text{tot}}^{h_{95}^{\text{SM}}} &\approx 0.0026 \text{ GeV}, \\ \text{BR}(h_{95}^{\text{SM}} \rightarrow \gamma\gamma) &\approx 1.4 \times 10^{-3}, \quad \text{BR}(h_{95}^{\text{SM}} \rightarrow b\bar{b}) \approx 0.81.\end{aligned}\tag{20}$$

Since top quark makes the dominant contributions to the Higgs production, the cross section for $gg \rightarrow h_{95}^{\text{NP}}$ and $\sigma(Z^* \rightarrow Zh_{95}^{\text{NP}})$ can be estimated by [21]

$$\begin{aligned}\sigma(gg \rightarrow h_{95}^{\text{NP}}) &\approx C_{h_{95}uu}^2 \sigma(gg \rightarrow h_{95}^{\text{SM}}), \\ \Gamma(h_{95}^{\text{NP}} \rightarrow ZZ^*) &\approx C_{h_{95}VV}^2 \Gamma(h_{95}^{\text{SM}} \rightarrow ZZ^*),\end{aligned}\tag{21}$$

where the coefficients $C_{h_{95}uu}$, $C_{h_{95}VV}$ are the normalized couplings of 95 GeV Higgs in NP models with up-quarks and gauge bosons respectively (in units of the corresponding SM couplings). The branch ratios for $h_{95}^{\text{NP}} \rightarrow \gamma\gamma$ or $b\bar{b}$ can be estimated by [21]

$$\begin{aligned}\text{BR}(h_{95}^{\text{NP}} \rightarrow \gamma\gamma) &\approx C_{h_{95}uu}^2 \text{BR}(h_{95}^{\text{SM}} \rightarrow \gamma\gamma) \frac{\Gamma_{\text{tot}}^{h_{95}^{\text{SM}}}}{\Gamma_{\text{tot}}^{h_{95}^{\text{NP}}}}, \\ \text{BR}(h_{95}^{\text{NP}} \rightarrow b\bar{b}) &\approx C_{h_{95}dd}^2 \text{BR}(h_{95}^{\text{SM}} \rightarrow b\bar{b}) \frac{\Gamma_{\text{tot}}^{h_{95}^{\text{SM}}}}{\Gamma_{\text{tot}}^{h_{95}^{\text{NP}}}},\end{aligned}\tag{22}$$

where the coefficients $C_{h_{95}dd}$ is the normalized couplings of 95 GeV Higgs in NP models with down-quarks, and [58]

$$\begin{aligned}\Gamma_{\text{tot}}^{h_{95}^{\text{NP}}} &\approx C_{h_{95}dd}^2 (\Gamma_{b\bar{b}}^{h_{95}^{\text{SM}}} + \Gamma_{\tau\bar{\tau}}^{h_{95}^{\text{SM}}}) + C_{h_{95}uu}^2 (\Gamma_{c\bar{c}}^{h_{95}^{\text{NP}}} + \Gamma_{gg}^{h_{95}^{\text{SM}}}) + C_{h_{95}VV}^2 \Gamma_{WW^*}^{h_{95}^{\text{SM}}}, \\ \text{BR}(h_{95}^{\text{SM}} \rightarrow \tau\tau) &\approx 0.082, \quad \text{BR}(h_{95}^{\text{SM}} \rightarrow c\bar{c}) \approx 0.037, \quad \text{BR}(h_{95}^{\text{SM}} \rightarrow gg) \approx 0.058, \\ \text{BR}(h_{95}^{\text{SM}} \rightarrow WW^*) &\approx 0.012.\end{aligned}\tag{23}$$

In the B-LSSM, we have

$$\begin{aligned}C_{h_{95}uu} = C_{h_{11}uu} &= Z_{h,12} \frac{v}{v_1}, \quad C_{h_{95}dd} = C_{h_{11}dd} = Z_{h,11} \frac{v}{v_1}, \\ C_{h_{95}VV} = C_{h_{11}VV} &= Z_{h,11} \frac{v_1}{v} + Z_{h,12} \frac{v_2}{v}.\end{aligned}\tag{24}$$

Particle Data Group collects various signal strengths of 125 GeV Higgs, where the results with high precision read [56]

$$\mu(h_{125})_{\gamma\gamma} = \frac{\sigma(gg \rightarrow h_{125}^{\text{NP}}) \text{BR}(h_{125}^{\text{NP}} \rightarrow \gamma\gamma)}{\sigma(gg \rightarrow h_{125}^{\text{SM}}) \text{BR}(h_{125}^{\text{SM}} \rightarrow \gamma\gamma)} = 1.10 \pm 0.06,$$

$$\begin{aligned}
\mu(h_{125})_{WW^*} &= \frac{\sigma(gg \rightarrow h_{125}^{\text{NP}}) \text{BR}(h_{125}^{\text{NP}} \rightarrow WW^*)}{\sigma(gg \rightarrow h_{125}^{\text{SM}}) \text{BR}(h_{125}^{\text{SM}} \rightarrow WW^*)} = 1.00 \pm 0.08, \\
\mu(h_{125})_{ZZ^*} &= \frac{\sigma(gg \rightarrow h_{125}^{\text{NP}}) \text{BR}(h_{125}^{\text{NP}} \rightarrow ZZ^*)}{\sigma(gg \rightarrow h_{125}^{\text{SM}}) \text{BR}(h_{125}^{\text{SM}} \rightarrow ZZ^*)} = 1.02 \pm 0.08, \\
\mu(h_{125})_{b\bar{b}} &= \frac{\Gamma(h_{125}^{\text{NP}} \rightarrow VV^*) \text{BR}(h_{125}^{\text{NP}} \rightarrow b\bar{b})}{\Gamma(h_{125}^{\text{SM}} \rightarrow VV^*) \text{BR}(h_{125}^{\text{SM}} \rightarrow b\bar{b})} = 0.99 \pm 0.12, \\
\mu(h_{125})_{\tau\bar{\tau}} &= \frac{\Gamma(h_{125}^{\text{NP}} \rightarrow VV^*) \text{BR}(h_{125}^{\text{NP}} \rightarrow \tau\bar{\tau})}{\Gamma(h_{125}^{\text{SM}} \rightarrow VV^*) \text{BR}(h_{125}^{\text{SM}} \rightarrow \tau\bar{\tau})} = 0.91 \pm 0.09,
\end{aligned} \tag{25}$$

and VV^* denotes WW^* or ZZ^* . Since top quark makes the dominant contributions to the Higgs production, $\sigma(gg \rightarrow h_{125}^{\text{NP}})$ and $\Gamma(h_{125}^{\text{NP}} \rightarrow VV^*)$ can be estimated by [21]

$$\begin{aligned}
\sigma(gg \rightarrow h_{125}^{\text{NP}}) &\approx C_{h_{125}uu}^2 \sigma(gg \rightarrow h_{125}^{\text{SM}}), \\
\Gamma(h_{125}^{\text{NP}} \rightarrow VV^*) &\approx C_{h_{125}VV}^2 \Gamma(h_{125}^{\text{SM}} \rightarrow VV^*),
\end{aligned} \tag{26}$$

where the coefficients $C_{h_{125}uu}$, $C_{h_{125}VV}$ are the normalized couplings of 125 GeV Higgs in NP models with up-quarks and gauge bosons respectively (in units of the corresponding SM couplings). For Higgs boson in the SM, we have

$$\begin{aligned}
\Gamma_{\text{tot}}^{h_{125}^{\text{SM}}} &\approx 0.0037 \text{ GeV}, \quad \text{BR}(h_{125}^{\text{SM}} \rightarrow b\bar{b}) \approx 0.53, \quad \text{BR}(h_{125}^{\text{SM}} \rightarrow WW^*) \approx 0.26, \\
\text{BR}(h_{125}^{\text{SM}} \rightarrow \tau\bar{\tau}) &\approx 0.06, \quad \text{BR}(h_{125}^{\text{SM}} \rightarrow ZZ^*) \approx 0.028, \quad \text{BR}(h_{125}^{\text{SM}} \rightarrow \gamma\gamma) \approx 0.0025.
\end{aligned} \tag{27}$$

The branch ratios for $h_{125}^{\text{NP}} \rightarrow \gamma\gamma$, $h_{125}^{\text{NP}} \rightarrow WW^*$, $h_{125}^{\text{NP}} \rightarrow ZZ^*$, $h_{125}^{\text{NP}} \rightarrow b\bar{b}$, $h_{125}^{\text{NP}} \rightarrow \tau\bar{\tau}$ can be estimated by

$$\begin{aligned}
\text{BR}(h_{125}^{\text{NP}} \rightarrow \gamma\gamma) &\approx C_{h_{125}uu}^2 \text{BR}(h_{125}^{\text{SM}} \rightarrow \gamma\gamma) \frac{\Gamma_{\text{tot}}^{h_{125}^{\text{SM}}}}{\Gamma_{\text{tot}}^{h_{125}^{\text{NP}}}}, \\
\text{BR}(h_{125}^{\text{NP}} \rightarrow VV^*) &\approx C_{h_{125}VV}^2 \text{BR}(h_{125}^{\text{SM}} \rightarrow VV^*) \frac{\Gamma_{\text{tot}}^{h_{125}^{\text{SM}}}}{\Gamma_{\text{tot}}^{h_{125}^{\text{NP}}}}, \\
\text{BR}(h_{125}^{\text{NP}} \rightarrow b\bar{b}) &\approx C_{h_{125}dd}^2 \text{BR}(h_{125}^{\text{SM}} \rightarrow b\bar{b}) \frac{\Gamma_{\text{tot}}^{h_{125}^{\text{SM}}}}{\Gamma_{\text{tot}}^{h_{125}^{\text{NP}}}}, \\
\text{BR}(h_{125}^{\text{NP}} \rightarrow \tau\bar{\tau}) &\approx C_{h_{125}dd}^2 \text{BR}(h_{125}^{\text{SM}} \rightarrow \tau\bar{\tau}) \frac{\Gamma_{\text{tot}}^{h_{125}^{\text{SM}}}}{\Gamma_{\text{tot}}^{h_{125}^{\text{NP}}}},
\end{aligned} \tag{28}$$

where the coefficients $C_{h_{125}dd}$ is the normalized couplings of 125 GeV Higgs in NP models with down-quarks, and

$$\Gamma_{\text{tot}}^{h_{125}^{\text{NP}}} \approx C_{h_{125}dd}^2 (\Gamma_{b\bar{b}}^{h_{125}^{\text{SM}}} + \Gamma_{\tau\bar{\tau}}^{h_{125}^{\text{SM}}}) + C_{h_{125}uu}^2 \Gamma_{\gamma\gamma}^{h_{125}^{\text{SM}}} + C_{h_{125}VV}^2 (\Gamma_{WW^*}^{h_{125}^{\text{SM}}} + \Gamma_{ZZ^*}^{h_{125}^{\text{SM}}}). \tag{29}$$

In the B-LSSM, we have

$$\begin{aligned} C_{h_{125}uu} &= C_{h_2uu} = Z_{h,22} \frac{v}{v_1}, \quad C_{h_{125}dd} = C_{h_2dd} = Z_{h,21} \frac{v}{v_1}, \\ C_{h_{125}VV} &= Z_{h,21} \frac{v_1}{v} + Z_{h,22} \frac{v_2}{v}. \end{aligned} \quad (30)$$

To carry out the numerical evaluations, we take the relevant SM input parameters as $m_W = 80.385$ GeV, $m_Z = 90.1876$ GeV, $\alpha_{em}(m_Z) = 1/128.9$, $\alpha_s(m_Z) = 0.118$. The measured SM-like Higgs mass is [56]

$$m_h = 125.09 \pm 0.24 \text{ GeV}. \quad (31)$$

Due to the introducing of $U(1)_{B-L}$ gauge group, a new Z' gauge boson is introduced in the B-LSSM. Refs. [59–61] give an upper bound on the ratio between the Z' mass $M_{Z'} \approx \frac{1}{2}g_B u$ and its gauge coupling at 99% CL as

$$M_{Z'}/g_B \geq 6 \text{ TeV}. \quad (32)$$

For simplicity, we take $g_B = 0.5$ in the following analysis, and Eq. (32) indicates $M_{Z'} \geq 3$ TeV in this case. As analyzed in Refs. [62, 63], the effects of new Z' in the B-LSSM on the couplings of Z -charged leptons which are measured at LEP precisely [56], can be eliminated by redefining the neutral currents involving charged leptons. It indicates that the redefined Z boson in the B-LSSM can coincide with the one measured at the LEP [56]. The LHC experimental data constrains $\tan \beta' < 1.5$ [64]. Based on the analysis about $\bar{B} \rightarrow X_s \gamma$ and $B_s^0 \rightarrow \mu^+ \mu^-$ in our previous work [65], we take $m_{H^\pm} = 1.5$ TeV. To coincide with the constraints from the direct searches of squarks, sgluon at the LHC [66, 67] and the observed Higgs signal analyzed in Ref. [68], we take $m_{\tilde{g}} = m_{\tilde{q}} = m_{\tilde{u}} = 2.5$ TeV for simplicity.

Firstly, we investigate the masses of the lightest and next-to-lightest Higgs bosons within the B-LSSM. Taking $g_{YB} = -0.4$, $M_{Z'} = 4.2$ TeV, $B_\eta = (1 \text{ TeV})^2$, we plot m_{h_i} versus $\tan \beta'$ for $A_t = 0.2$ TeV in Fig. 1 (a), and m_{h_i} versus A_t for $\tan \beta' = 1.075$ in Fig. 1 (b). Where the black, red lines denote the results for m_{h_1} , m_{h_2} respectively, the solid, dashed, dotted lines denote the results for $\tan \beta = 5, 15, 25$ respectively, the green areas denote the range $94 \text{ GeV} < m_{h_i} < 96 \text{ GeV}$, the gray areas denote the range $124 \text{ GeV} < m_{h_i} < 126 \text{ GeV}$. It can be noted from the picture that $\tan \beta'$, $\tan \beta$ and A_t affect the two light Higgs boson

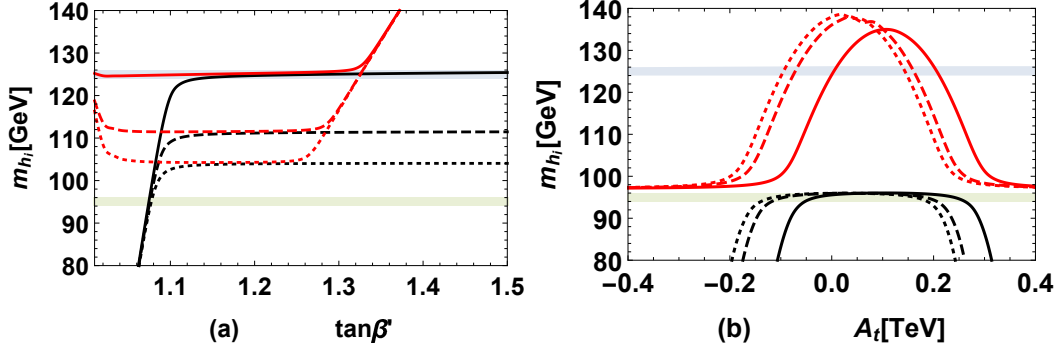


FIG. 1: Taking $g_{YB} = -0.4$, $M_{Z'} = 4.2$ TeV, $B_\eta = (1 \text{ TeV})^2$, m_{h_i} versus $\tan \beta'$ for $A_t = 0.2$ TeV is plotted in (a), and m_{h_i} versus A_t for $\tan \beta' = 1.075$ is plotted in (b). The black, red lines denote the results for m_{h_1} , m_{h_2} respectively, the solid, dashed, dotted lines denote the results for $\tan \beta = 5, 15, 25$ respectively, the green areas denote the range $94 \text{ GeV} < m_{h_i} < 96 \text{ GeV}$, the gray areas denote the range $124 \text{ GeV} < m_{h_i} < 126 \text{ GeV}$.

masses obviously. Importantly, both the 95 GeV Higgs and the SM-like Higgs with a mass of 125 GeV are attainable within the B-LSSM. Fig. 1 (a) demonstrates that $\tan \beta'$ is constrained strictly for $m_{h_1} \approx 95$ GeV in our chosen parameter space, and the effects of $\tan \beta'$ on m_{h_i} ($i = 1, 2$) are influenced significantly by the value of $\tan \beta$. This fact can be seen explicitly in Eq. (16). From Fig. 1 (b), we can see that A_t is subject to a strict limitation through the requirement of setting $m_{h_2} \approx 125$ GeV.

As shown in Eq. (16), the lightest Higgs boson is dominated by one of the B-LSSM specific Higgs states, and B_η , g_{YB} , $M_{Z'}$ can affect the theoretical predictions on the two light Higgs boson masses significantly. Then we take $\tan \beta' = 1.075$, $\tan \beta = 5$, $A_t = 0.2$ TeV and plot m_{h_i} versus B_η for $M_{Z'} = 4.2$ TeV in Fig. 2 (a), and m_{h_i} versus $M_{Z'}$ for $B_\eta = (1 \text{ TeV})^2$ in Fig. 2 (b). Where the black, red lines denote the results for m_{h_1} , m_{h_2} respectively, the solid, dashed, dotted lines denote the results for $g_{YB} = -0.8, -0.4, 0$ respectively, the green areas denote the range $94 \text{ GeV} < m_{h_i} < 96 \text{ GeV}$, the gray areas denote the range $124 \text{ GeV} < m_{h_i} < 126 \text{ GeV}$.

Fig. 2 (a) shows that both m_{h_1} and m_{h_2} increase as B_η increases, and the dotted lines intersect because there is no mixing effects between the SM-like Higgs with the B-LSSM

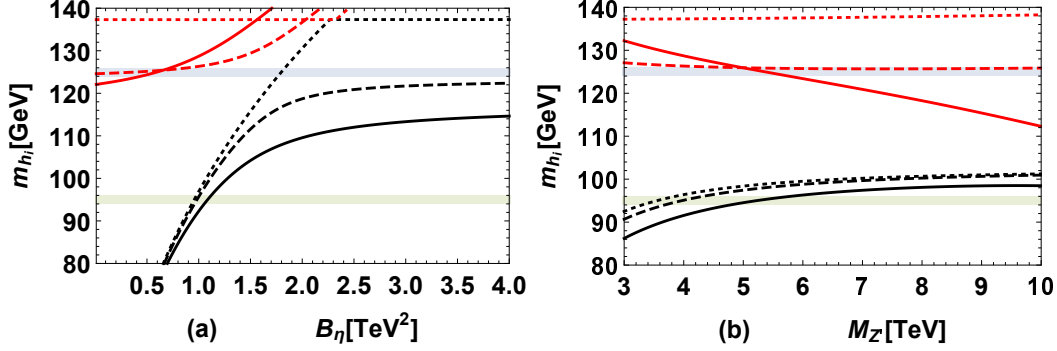


FIG. 2: Taking $\tan \beta' = 1.075$, $\tan \beta = 5$, $A_t = 0.2$ TeV, m_{h_i} versus B_{η} for $M_{Z'} = 4.2$ TeV is plotted in (a), and m_{h_i} versus $M_{Z'}$ for $B_{\eta} = (1 \text{ TeV})^2$ is plotted in (b). The black, red lines denote the results for m_{h_1} , m_{h_2} respectively, the solid, dashed, dotted lines denote the results for $g_{YB} = -0.8, -0.4, 0$ respectively, the green areas denote the range $94 \text{ GeV} < m_{h_i} < 96 \text{ GeV}$, the gray areas denote the range $124 \text{ GeV} < m_{h_i} < 126 \text{ GeV}$.

specific Higgs states at the tree level when $g_{YB} = 0$ (the fact can be seen obviously in Eq. (15)). In addition, h_2 is primarily governed by the SM-like Higgs state and m_{h_2} does not depend on the value of B_{η} . Conversely, m_{h_1} is dominated by the B-LSSM specific Higgs state and rises with increasing B_{η} . As B_{η} increases, the mass of the B-LSSM specific Higgs state surpasses the mass of the SM-like Higgs state, causing h_1 to be dominated by the SM-like Higgs state and h_2 to be dominated by the B-LSSM specific Higgs state. This situation results in the intersection of the two dotted lines in Fig. 2 (a). The three red lines in Fig. 2 (b) show that $M_{Z'}$ affects m_{h_2} obviously when $g_{YB} = -0.8$, because the mixing effects between the SM-like Higgs with the B-LSSM specific Higgs states are large for large g_{YB} and play important roles on SM-like Higgs boson masses.

Based on the preceding analysis, it is evident that both the 95 GeV Higgs boson and the 125 GeV SM-like Higgs boson are attainable in the B-LSSM. Due to the masses of the two light Higgs bosons are influenced significantly in a complex manner by $\tan \beta$, $\tan \beta'$, A_t , B_{η} , g_{YB} , $M_{Z'}$, we scan the following parameter space

$$\begin{aligned} \tan \beta &= (2, 40), \tan \beta' = (1, 1.5), A_t = (-1, 1) \text{ TeV}, \\ B_{\eta} &= (0.1^2, 2^2) \text{ TeV}^2, g_{YB} = (-1, 0), M_{Z'} = (3, 10) \text{ TeV}, \end{aligned} \quad (33)$$

Observables	O_i^{th}	O_i^{exp}	Deviations in %
m_{h_1} [GeV]	94.83	95.00	0.12
m_{h_2} [GeV]	125.07	125.09	0.02
$\mu(h_{125})_{\gamma\gamma}$	1.04	1.10	5.45
$\mu(h_{125})_{WW^*}$	1.04	1.00	6.00
$\mu(h_{125})_{ZZ^*}$	1.04	1.02	1.96
$\mu(h_{125})_{b\bar{b}}$	0.83	0.99	16.16
$\mu(h_{125})_{\tau\bar{\tau}}$	0.83	0.91	8.79
$\mu(h_{95})_{\gamma\gamma}$	0.11	0.33	66.67
$\mu(h_{95})_{b\bar{b}}$	0.09	0.117	23.08

TABLE I: The results obtained for the best fit corresponding to $\chi^2 = \mathbf{1.5}$.

to comprehensively explore the collective influences of $\tan\beta$, $\tan\beta'$, A_t , B_η , g_{YB} , $M_{Z'}$ on the Higgs signal strengths. To explore the best fit describing 125 GeV Higgs mass and the diphoton, $b\bar{b}$ excesses, a χ^2 test is performed. The χ^2 function can be constructed as

$$\chi^2 = \sum_i \left(\frac{O_i^{\text{th}} - O_i^{\text{exp}}}{\sigma_i^{\text{exp}}} \right)^2, \quad (34)$$

where O_i^{th} denotes the i -th observable computed theoretically, O_i^{exp} is the corresponding experimental value and σ_i^{exp} is the uncertainty in O_i^{exp} .

Scanning the parameter space in Eq. (33) and keeping $94 \text{ GeV} < m_{h_1} < 96 \text{ GeV}$, $124 \text{ GeV} < m_{h_2} < 126 \text{ GeV}$ in the scanning, we plot the allowed ranges of $A_t - \tan\beta$, $B_\eta - \tan\beta'$, $M_{Z'} - g_{YB}$ in Fig. 3 (a), Fig. 3 (b), Fig. 3 (c) respectively, and the obtained $\mu(h_{95})_{\gamma\gamma} - \mu(h_{95})_{b\bar{b}}$ in Fig. 3 (d). In Fig. 3, the gray points denote the results excluded by considering the $\mu(h_{95})_{\gamma\gamma}$, $\mu(h_{95})_{b\bar{b}}$ in the experimental 2σ intervals, the red points denote the results excluded by considering the 125 GeV Higgs signal strengths in the experimental 2σ intervals, and the green points denote the results with $\mu(h_{95})_{\gamma\gamma}$, $\mu(h_{95})_{b\bar{b}}$ and the 125 GeV Higgs signal strengths in the experimental 2σ intervals. The ‘black stars’ denote the best fit corresponding to $\chi^2 = 1.5$ with the diphoton excess in Eq. (3), $b\bar{b}$ excess in Eq. (4), 125 GeV Higgs mass in Eq. (31), and 125 GeV Higgs signal strengths in Eq. (25). The results of the best fit are listed in Tab. I. The deviations listed in Tab. I indicates that the signal strengths

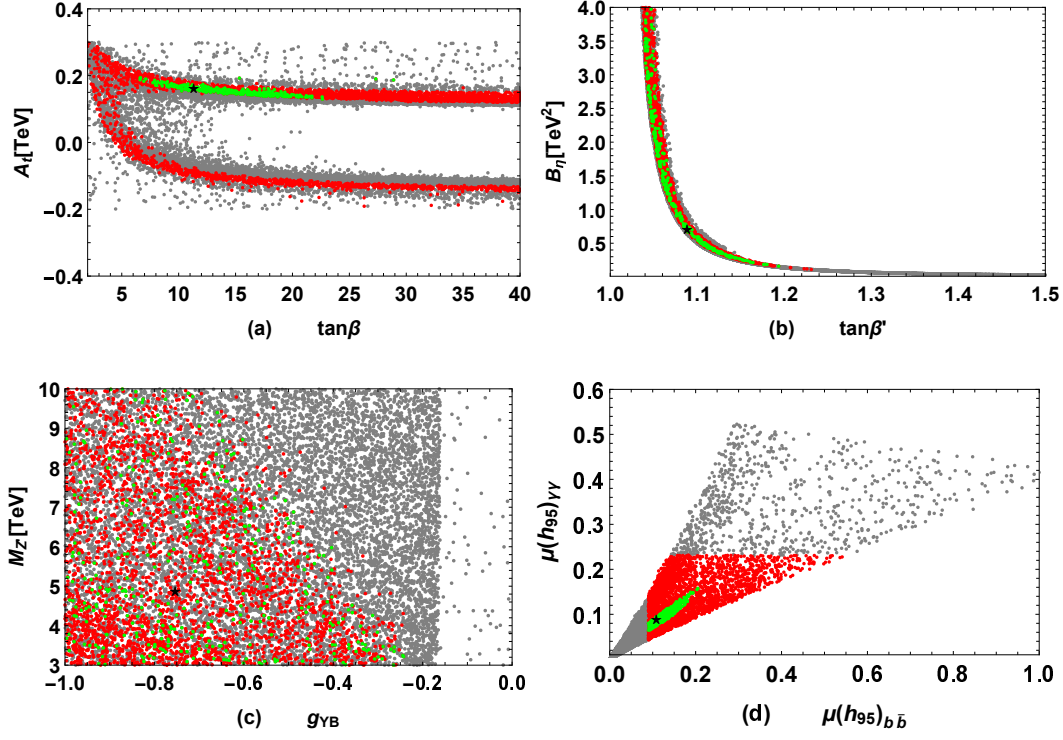


FIG. 3: Scanning the parameter space in Eq. (33) and keeping $94 \text{ GeV} < m_{h_1} < 96 \text{ GeV}$, $124 \text{ GeV} < m_{h_2} < 126 \text{ GeV}$ in the scanning, the allowed ranges of $A_t - \tan\beta$ (a), $B_\eta - \tan\beta'$ (b), $M_{Z'} - g_{YB}$ (c) and the obtained $\mu(h_{95})_{\gamma\gamma} - \mu(h_{95})_{b\bar{b}}$ (d) are plotted. The ‘black stars’ denote the best fit corresponding to $\chi^2 = 1.5$, the gray points denote the results excluded by considering the $\mu(h_{95})_{\gamma\gamma}$, $\mu(h_{95})_{b\bar{b}}$ in the experimental 2σ intervals, the red points denote the results excluded by considering the 125 GeV Higgs signal strengths in the experimental 2σ intervals, and the green points denote the results with $\mu(h_{95})_{\gamma\gamma}$, $\mu(h_{95})_{b\bar{b}}$ and the 125 GeV Higgs signal strengths in the experimental 2σ intervals.

predicted in the B-LSSM are hard to fit the observed results in Eq. (4) and Eq. (25) in the experimental 1σ intervals, but can fit the observed results in the experimental 2σ intervals. Hence, the high-precision observations of $\mu(h_{95})_{\gamma\gamma}$ and $\mu(h_{95})_{b\bar{b}}$ in future may exclude the B-LSSM, or further constraint the parameter space of the model.

Fig. 3 (a) shows that negative A_t is excluded by considering the signal strengths of two

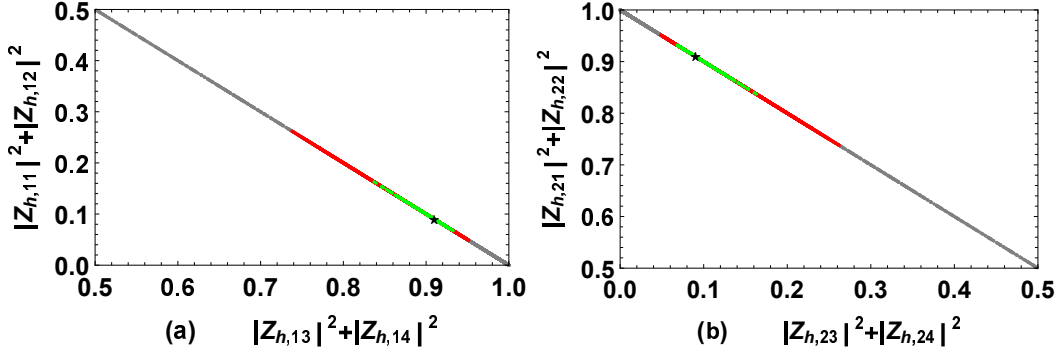


FIG. 4: Scanning the parameter space in Eq. (33) and keeping $94 \text{ GeV} < m_{h_1} < 96 \text{ GeV}$, $124 \text{ GeV} < m_{h_2} < 126 \text{ GeV}$ in the scanning, the results of $|Z_{h,11}|^2 + |Z_{h,12}|^2$ versus $|Z_{h,13}|^2 + |Z_{h,14}|^2$ (a), $|Z_{h,21}|^2 + |Z_{h,22}|^2$ versus $|Z_{h,23}|^2 + |Z_{h,24}|^2$ (b) are plotted. The ‘black stars’ denote the best fit corresponding to $\chi^2 = 1.5$, the gray points denote the results excluded by considering the $\mu(h_{95})_{\gamma\gamma}$, $\mu(h_{95})_{b\bar{b}}$ in the experimental 2σ intervals, the red points denote the results excluded by considering the 125 GeV Higgs signal strengths in the experimental 2σ intervals, and the green points denote the results with $\mu(h_{95})_{\gamma\gamma}$, $\mu(h_{95})_{b\bar{b}}$ and the 125 GeV Higgs signal strengths in the experimental 2σ intervals.

light Higgs bosons in the experimental 2σ intervals, and most of A_t are excluded by the conditions $94 \text{ GeV} < m_{h_1} < 96 \text{ GeV}$, $124 \text{ GeV} < m_{h_2} < 126 \text{ GeV}$. The two light Higgs masses prefer large B_η for small $\tan\beta'$ and B_η is limited strictly for given $\tan\beta'$ as shown in Fig. 3 (b), because B_η , $\tan\beta'$ affect the two light Higgs boson masses significantly as shown in Eq. (16). In addition, $\tan\beta'$ is limited in the range $1.04 \lesssim \tan\beta' \lesssim 1.16$ by considering the two light Higgs signal strengths in the experimental 2σ intervals. Fig. 3 (c) shows that g_{YB} is limited in the range $g_{YB} \lesssim -0.3$ and $M_{Z'}/|g_{YB}| \lesssim 16.5 \text{ TeV}$ by considering the two light Higgs signal strengths in the experimental 2σ intervals, which provides a new bound on the ratio of Z' boson mass with the kinetic mixing parameter g_{YB} if the diphoton and $b\bar{b}$ excesses are verified in future.

In order to show explicitly the components of the two light Higgs bosons, we plot the results of $|Z_{h,11}|^2 + |Z_{h,12}|^2$ versus $|Z_{h,13}|^2 + |Z_{h,14}|^2$ in Fig. 4 (a), and $|Z_{h,21}|^2 + |Z_{h,22}|^2$ versus $|Z_{h,23}|^2 + |Z_{h,24}|^2$ in Fig. 4 (b). The definitions of the ‘black stars’, gray points, green points,

red points are same to the ones of Fig. 3. It can be found from the picture that the lightest 95 GeV Higgs is dominated by the new Higgs singlets introduced in the B-LSSM, while the next-to-lightest 125 GeV Higgs is dominated by the two Higgs doublets. In addition, it is obvious that the mixing effects between Higgs doublets with B-LSSM specific scalar singlets play important roles in explaining the diphoton and $b\bar{b}$ excesses at about 95 GeV, i.e. considering the two loop effective potential corrections is valuable in calculating the two light Higgs boson masses and the scalar mixing effects.

In conclusion, the numerical results indicate the B-LSSM is hard to fit these signal strengths in the experimental 1σ intervals, but the model can reproduce the 125 GeV Higgs signal strengths, and the diphoton, $b\bar{b}$ excesses in the experimental 2σ intervals simultaneously. In addition, the high-precision observations of $\mu(h_{95})_{\gamma\gamma}$ and $\mu(h_{95})_{b\bar{b}}$ in future may exclude the B-LSSM or further support the Higgs sector in the B-LSSM, and considering the two loop effective potential corrections to the squared Higgs mass matrix is important to account for the mixing effects among Higgs sector.

Acknowledgments

The work has been supported by the National Natural Science Foundation of China (NNSFC) with Grants No. 12075074, No. 12235008, Hebei Natural Science Foundation for Distinguished Young Scholars with Grant No. A2022201017, No. A2023201041, Natural Science Foundation of Guangxi Autonomous Region with Grant No. 2022GXNSFDA035068, and the youth top-notch talent support program of the Hebei Province.

-
- [1] [CMS], CMS-PAS-HIG-14-037.
 - [2] A. M. Sirunyan *et al.* [CMS], Phys. Lett. B **793**, 320-347 (2019).
 - [3] C. Arcangeletti. on behalf of ATLAS collaboration, LHC Seminar, 7th of June, 2023.
 - [4] [ATLAS], ATLAS-CONF-2018-025.
 - [5] A. Tumasyan *et al.* [CMS], JHEP **07**, 073 (2023).
 - [6] [CMS], CMS-PAS-HIG-20-002.

- [7] R. Barate *et al.* [LEP Working Group for Higgs boson searches, ALEPH, DELPHI, L3 and OPAL], Phys. Lett. B **565**, 61-75 (2003).
- [8] S. Moretti and S. Munir, Eur. Phys. J. C **47**, 791-803 (2006).
- [9] U. Ellwanger, Phys. Lett. B **698**, 293-296 (2011).
- [10] J. Cao, Z. Heng, T. Liu and J. M. Yang, Phys. Lett. B **703**, 462-468 (2011).
- [11] D. Albornoz Vasquez, G. Belanger, C. Boehm, J. Da Silva, P. Richardson and C. Wymant, Phys. Rev. D **86**, 035023 (2012).
- [12] U. Ellwanger and C. Hugonie, Adv. High Energy Phys. **2012**, 625389 (2012).
- [13] F. Boudjema and G. D. La Rochelle, Phys. Rev. D **86**, 115007 (2012).
- [14] K. Schmidt-Hoberg and F. Staub, JHEP **10**, 195 (2012).
- [15] M. Badziak, M. Olechowski and S. Pokorski, JHEP **06**, 043 (2013).
- [16] M. Badziak, M. Olechowski and S. Pokorski, PoS **EPS-HEP2013**, 257 (2013).
- [17] R. Barbieri, D. Buttazzo, K. Kannike, F. Sala and A. Tesi, Phys. Rev. D **88**, 055011 (2013).
- [18] J. W. Fan, J. Q. Tao, Y. Q. Shen, G. M. Chen, H. S. Chen, S. Gascon-Shotkin, M. Lethuillier, L. Sgandurra and P. Soulet, Chin. Phys. C **38**, 073101 (2014).
- [19] C. T. Potter, Eur. Phys. J. C **76**, no.1, 44 (2016).
- [20] U. Ellwanger and M. Rodriguez-Vazquez, JHEP **02**, 096 (2016).
- [21] J. Cao, X. Guo, Y. He, P. Wu and Y. Zhang, Phys. Rev. D **95**, no.11, 116001 (2017).
- [22] J. Cao, X. Jia, Y. Yue, H. Zhou and P. Zhu, Phys. Rev. D **101**, no.5, 055008 (2020).
- [23] J. Cao, X. Jia, J. Lian and L. Meng, Phys. Rev. D **109**, no.7, 075001 (2024).
- [24] J. Cao, X. Jia and J. Lian, Phys. Rev. D **110**, no.11, 115039 (2024).
- [25] T. Biekötter, M. Chakraborti and S. Heinemeyer, Eur. Phys. J. C **80**, no.1, 2 (2020).
- [26] T. Biekötter and M. O. Olea-Romacho, JHEP **10**, 215 (2021).
- [27] T. Biekötter, A. Grohsjean, S. Heinemeyer, C. Schwanenberger and G. Weiglein, Eur. Phys. J. C **82**, no.2, 178 (2022).
- [28] S. Heinemeyer, C. Li, F. Lika, G. Moortgat-Pick and S. Paasch, Phys. Rev. D **106**, no.7, 075003 (2022).
- [29] T. Biekötter, S. Heinemeyer and G. Weiglein, JHEP **08**, 201 (2022).
- [30] T. Biekötter, S. Heinemeyer and G. Weiglein, Eur. Phys. J. C **83**, no.5, 450 (2023).

- [31] T. Biekötter, S. Heinemeyer and G. Weiglein, Phys. Lett. B **846**, 138217 (2023).
- [32] D. Azevedo, T. Biekötter and P. M. Ferreira, JHEP **11**, 017 (2023).
- [33] J. A. Aguilar-Saavedra, H. B. Câmara, F. R. Joaquim and J. F. Seabra, [arXiv:2307.03768 [hep-ph]].
- [34] D. Sachdeva and S. Sadhukhan, Phys. Rev. D **101**, no.5, 055045 (2020).
- [35] T. Biekötter, S. Heinemeyer and C. Muñoz, Eur. Phys. J. C **78**, no.6, 504 (2018).
- [36] T. Biekötter, S. Heinemeyer and C. Muñoz, Eur. Phys. J. C **79**, no.8, 667 (2019).
- [37] S. Ashanujjaman, S. Banik, G. Coloretti, A. Crivellin, B. Mellado and A. T. Mulaudzi, [arXiv:2306.15722 [hep-ph]].
- [38] A. Azatov, R. Contino and J. Galloway, JHEP **04**, 127 (2012).
- [39] S. Heinemeyer and T. Stefaniak, PoS **CHARGED2018**, 016 (2019).
- [40] S. Khalil and H. Okada, Phys. Rev. D **79**, 083510 (2009).
- [41] A. Elsayed, S. Khalil and S. Moretti, Phys. Lett. B **715**, 208-213 (2012).
- [42] A. Elsayed, S. Khalil, S. Moretti and A. Moursy, Phys. Rev. D **87**, no.5, 053010 (2013).
- [43] W. Abdallah, A. Hammad, S. Khalil and S. Moretti, Phys. Rev. D **95**, no.5, 055019 (2017).
- [44] S. Khalil and S. Moretti, Rept. Prog. Phys. **80**, no.3, 036201 (2017).
- [45] L. Delle Rose, S. Khalil, S. J. D. King, S. Kulkarni, C. Marzo, S. Moretti and C. S. Un, JHEP **07**, 100 (2018).
- [46] J. L. Yang, T. F. Feng and H. B. Zhang, J. Phys. G **47**, no.5, 055004 (2020).
- [47] J. L. Yang, H. B. Zhang, C. X. Liu, X. X. Dong and T. F. Feng, JHEP **08**, 086 (2021).
- [48] A. A. Abdelalim, B. Das, S. Khalil and S. Moretti, Nucl. Phys. B **985**, 116013 (2022).
- [49] S. Khalil, LHEP **2023**, 454 (2023).
- [50] S. Iguro, T. Kitahara and Y. Omura, Eur. Phys. J. C **82**, no.11, 1053 (2022).
- [51] J. L. Yang, T. F. Feng, Y. L. Yan, W. Li, S. M. Zhao and H. B. Zhang, Phys. Rev. D **99**, no.1, 015002 (2019).
- [52] R. J. Zhang, Phys. Lett. B **447**, 89-97 (1999).
- [53] J. R. Espinosa and R. J. Zhang, JHEP **03**, 026 (2000).
- [54] G. Degrandi, P. Slavich and F. Zwirner, Nucl. Phys. B **611**, 403-422 (2001).
- [55] G. Degrandi and P. Slavich, Nucl. Phys. B **825**, 119-150 (2010).

- [56] S. Navas *et al.* [Particle Data Group], Phys. Rev. D **110**, no.3, 030001 (2024).
- [57] P. Bechtle, H. E. Haber, S. Heinemeyer, O. Stål, T. Stefaniak, G. Weiglein and L. Zeune, Eur. Phys. J. C **77**, 67 (2017).
- [58] A. Djouadi, J. Kalinowski and M. Spira, Comput. Phys. Commun. **108**, 56-74 (1998).
- [59] ATLAS Collaboration, Report No. ATLAS-CONF-2016-045.
- [60] G. Cacciapaglia, C. Csaki, G. Marandella, and A. Strumia, Phys.Rev. D **74**, 033011 (2006) [hep-ph/0604111] .
- [61] M. Carena, A. Daleo, B. A. Dobrescu and T. M. P. Tait, Phys. Rev. D **70**, 093009 (2004) [hep-ph/0408098].
- [62] G. Cacciapaglia, C. Csaki, G. Marandella and A. Strumia, Phys. Rev. D **74**, 033011 (2006).
- [63] J. L. Yang, Z. F. Ge, X. Y. Yang, S. K. Cui and T. F. Feng, Chin. Phys. C **48**, no.11, 113102 (2024).
- [64] Lorenzo Basso, Adv. High Energy Phys. **2015**, 12 (2015).
- [65] J. L. Yang, T. F. Feng, H. B. Zhang, R. F. Zhu and S. M. Zhao, Eur. Phys. J. C **78**, 714 (2018).
- [66] ATLAS Collab., Phys. Rev. D **87**, 012008 (2013).
- [67] CMS Collab., JHEP **1210**, 018 (2012).
- [68] C. S. Un and O. Ozdal, Phys. Rev. D **93**, 055024 (2016) [arXiv:1601.02494 [hep-ph]].